



## A FULLY REVERSIBLE AXIAL FAN WITH TWO CONTRA-ROTATING IMPELLERS

Konrad BAMBERGER, Maximilian KLENK<sup>1</sup>, Thomas CAROLUS<sup>2</sup>

<sup>1</sup>University of Siegen, Institute for Fluid- and Thermodynamics, Germany

<sup>2</sup>Steinbeis-Transferzentrum FLOWTRANS, 57250 Netphen, Germany

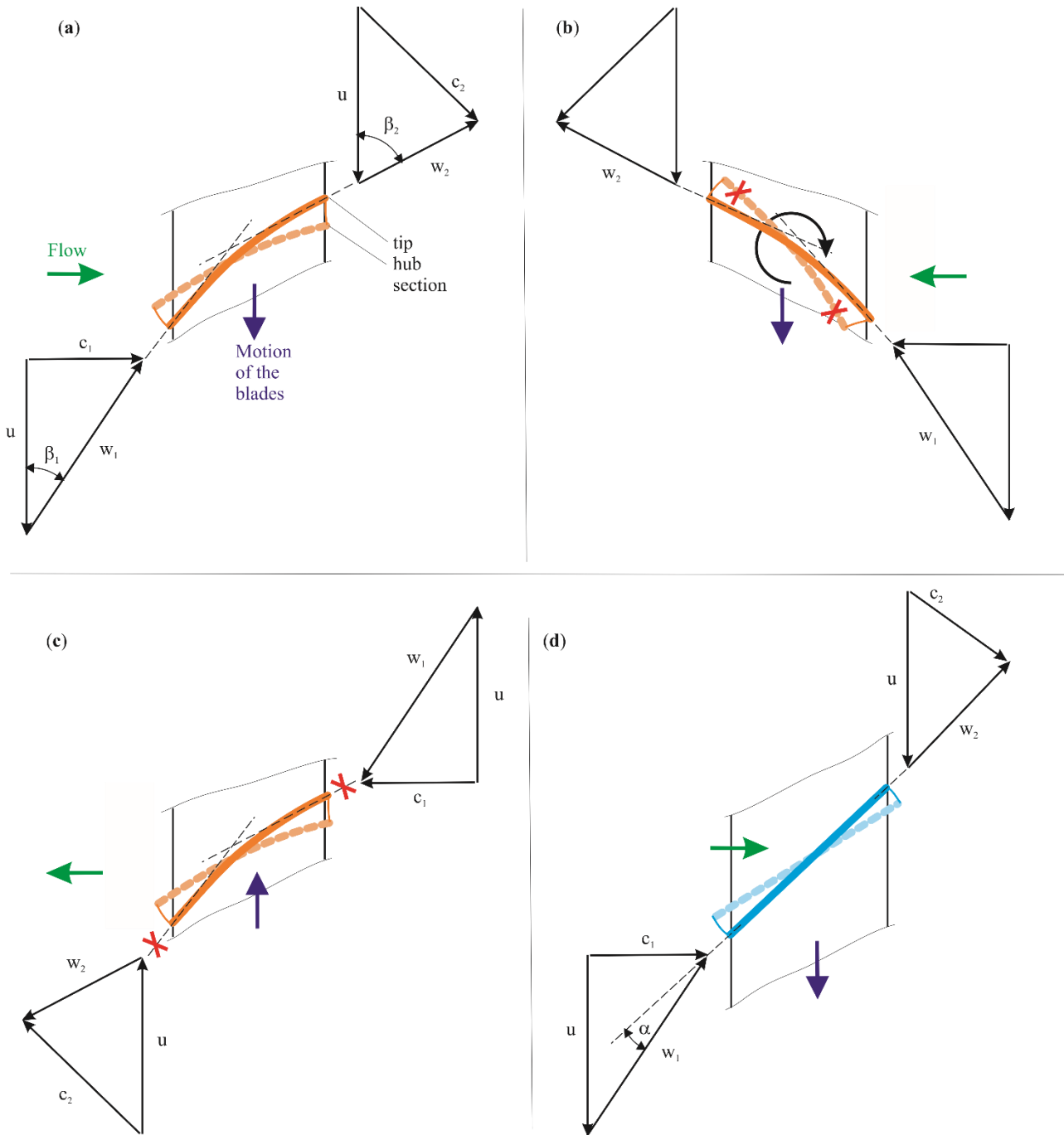
### SUMMARY

The objective of this paper is the design, manufacture and test of a fully reversible axial fan. The fundamental layout of the fan chosen consists of two identical contra-rotating impellers without guide vanes, placed in mirror image to each other in a duct-type housing. Given a fixed flow coefficient, a CFD-based optimization method is utilized to find the pressure rise coefficient, the rotational speed ratio of both impellers and the spanwise distributions of blade chord length and stagger angle that promise maximum total-to-static efficiency of the fully reversible fan. As a result, the impeller blades are composed of thin non-cambered airfoil elements, fully symmetric to the stagger line. They are twisted. The predicted optimal rotational speed of the downstream impeller is 82.5 % of the upstream impeller. For the design flow coefficient  $\phi = 0.10$  the optimal total-to-static pressure rise coefficient is  $\psi_{ts} = 0.5$ . These are typical values for a high pressure axial fan. For experimental validation two 80 mm diameter impellers were manufactured via 3D printing and mounted in a precision aluminum tube via three circular struts. The measured performance characteristics for a range of the impeller speed ratio confirm the prediction fairly well. The best total-to-static efficiency performance corresponds to a fan exit flow without swirl, which is achieved around the optimal rotational speed ratio of 0.825 to 1.0.

**Keywords:** reversible fan, axial, contra-rotating, optimization, multistage

### INTRODUCTION

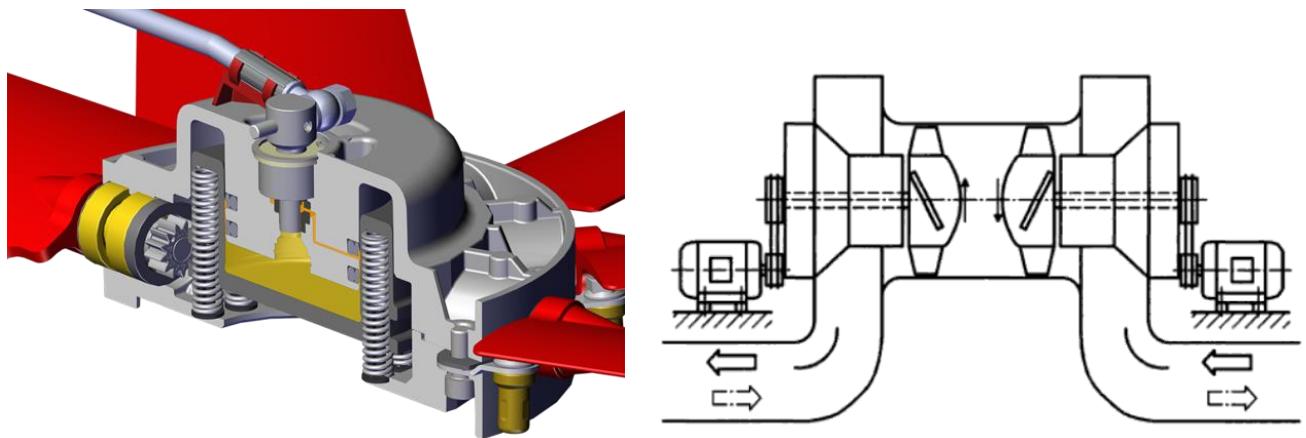
Some technical applications require a *fully* reversible fan. That means that the fan performance characteristics must be *identical* for both flow directions. Several design principles are known for both, centrifugal and axial reversible fans. As this work exclusively targets at the *axial* fan type, Fig. 1 depicts several options for a reversible axial blade cascades.



**Figure. 1:** (a) Baseline: Circular-arc cambered blade; (b) Blade turned by approx. 90°, reversed flow in spite of same direction of rotational speed - red crosses indicate mismatch of blade angles; (c) Reversed direction of rotational speed: reversed flow direction; red crosses indicate that inlet- and outlet angle are different from baseline, i.e. no full reversibility; (d) Non-cambered blade, allowing full reversibility at reversed rotational speed; the non-cambered blade requires an angle of attack  $\alpha > 0^\circ$ .

If the direction of rotational speed is required to stay untouched, the blades may be collectively turned (pitched) along their stacking lines by approx. 90°, Fig. 1(b). The principle design is analogous to the well-known variable pitch propeller. The inherent aerodynamic disadvantage is that the blade twist distribution is incorrect for the pitched blades. One way out is choosing a non-twisted blade design with its aerodynamic drawbacks, especially for impellers with low hub/tip diameter

ratio. A commercially available fan for agricultural machines, where the matrix of the engine cooling radiator has to be cleaned from dust regularly, is depicted in Fig. 2.



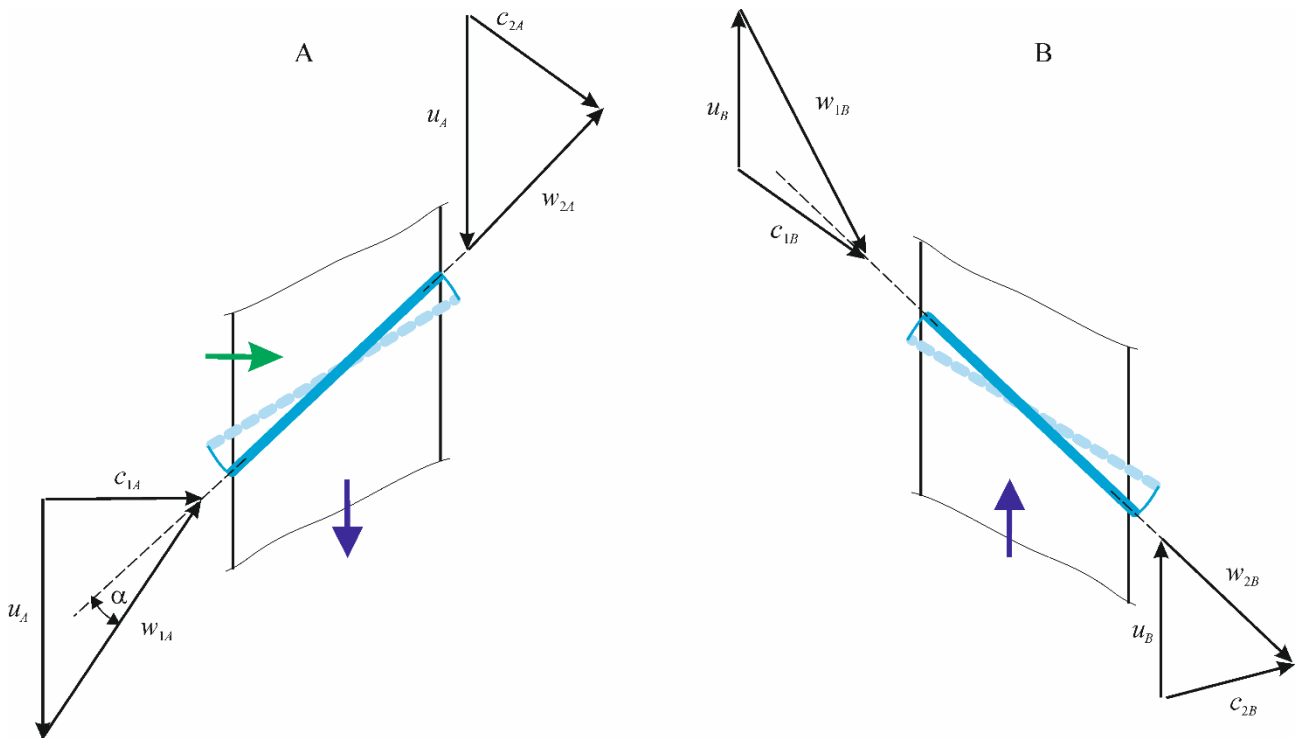
**Figure 2:** (Left): Fan impeller with hub allowing for approx. 90° turning of the blades and hence reversed flow without changing the direction of rotation [1]; (Right): Reversible axial fan assembly with two contra-rotating impellers, German patent DE 3938975 C1 [2].

Fig. 1(c) illustrates the problem when reversed flow direction is provided by just reversing the direction of rotational speed of the impeller. The blade camber is wrong and the blade angles are different from the baseline. This prevents full reversibility. In contrast, if the camber is removed, i.e. each blade section is made of a non-cambered flat plate, full symmetry and thus full reversibility of the fan are achieved, Fig. 1(d). A flat plate, however, produces relatively low lift (coefficients) at high drag-to-lift ratios which is, for instance, documented in Eck [3]. A non-cambered blade can provide lift only if the inflow meets the blade with an angle of attack  $\alpha > 0^\circ$  which, however, is limited due to the risk of stall. Eventually, this results in a small flow deflection and hence pressure rise of the fan and a low efficiency. Fig. 3 depicts a contra-rotating configuration. If the direction of each impeller is reversed, the flow direction is also reversed. The non-cambered blades ensure full reversibility. Naturally, the pressure rise is increased as compared to the single-impeller design. The lower Fig. 2 shows a fan assembly accordingly as patented in the German patent DE 3938975 C1 [2] from 1989. In this patent specification more historic references concerning fully reversible fans are presented.

The objective of this study is the design of a fully reversible fan consisting of two identical yet mirrored contra-rotating impellers with non-cambered but twisted blades. Guide vanes shall be excluded. A typical application is the decentralized room ventilation. Therefore, as an example, a *small* fan is designed and investigated in this study. The method and the conclusions, however, are applicable to any other fan size. Fig. 3 reveals some of the questions and challenges. For maximum (total-to-static) efficiency

- What is the most suitable pressure rise coefficient?
- Which is the optimal ratio of rotational speed of both impellers?
- Which is the optimal spanwise blade stagger angle and chord length distribution for the upstream and mirrored downstream impeller?
- Which is the optimal hub-to-tip ratio?

During the course of this study a CFD-based optimization method is utilized to identify these parameters. Then a prototype is manufactured and the predictions of the optimization are validated experimentally.



**Figure 3:** Two contra-rotating non-cambered blades, downstream blade is mirrored; full reversibility because inlet/outlet angle are identical for reversed rotational speeds and hence flow direction. In general, the rotational speed and hence the circumferential velocities  $u$  can be different for A and B, but  $c_{1B}$  always equals  $c_{2A}$ .

## OPTIMIZATION STRATEGY

### Optimization Target and Algorithm

Objective of the optimization is the maximum total-to-static efficiency at a given flow rate. Due to the desired feature “full reversibility” a set of geometrical constraints exists, but there is no constraint with respect to pressure rise. I.e., the optimization strategy targets at a design that is best-suited for maximum efficiency – the corresponding pressure rise of the machine is an outcome of the optimization.

The objective function is evaluated by CFD simulations. Although the comparison of CFD results to the experimental data will show good agreement (see Chapter 4), the CFD model is still unsuitable to reliably compute the gradient of the objective function by the method of finite differences. Hence, gradient-based optimization algorithms are not adequate for the present study. It was eventually decided to use the more robust Simplex method by Nelder and Mead [4], despite its known weaknesses with respect to speed of convergence.

### Optimization Parameters

- Constraints to guarantee full reversibility of the symmetric contra-rotating fan  
 In order to obtain equal flow conditions in regular and reverse operation, the blade sections must be point-symmetric with respect to the center of gravity. In principle, this constraint does not exclude cambered blade sections. However, as shown earlier, aerodynamically adequate camber will never comply with this constraint. Hence non-cambered sections were used. These blade sections must be stacked on a straight line pointing in radial direction. In other words, skewed or swept blades are prohibitive.

- Fixed parameters

- The design flow rate is set to  $Q = 32 \text{ m}^3/\text{h}$ . In order to match this flow rate with an adequate value of the non-dimensional flow coefficient

$$\phi \equiv Q / \left( \frac{\pi^2}{4} D^3 n_A \right), \quad (1)$$

here the typical value for an axial fan  $\phi = 0.1055$ , the nominal impeller diameter and the rotational speed are fixed to  $D = 80 \text{ mm}$  and  $n_A = 4000 \text{ rpm}$ , respectively. Note that  $n_A$  is the rotational speed of the upstream impeller. The speed of the second impeller can be different which will also affect the value of the flow coefficient.

- It was decided to use blades of constant thickness although full reversibility would allow a variable thickness distribution over the chord length. The reason is well known: From an aerodynamic point of view, the thickness should be as small as possible. However, there is always a minimal allowable thickness to ensure structural strength and manufacturability. In the present study, the thickness was set to 0.5 mm. The blade sections were rounded at leading and trailing edge.
- The number of blades was fixed to eight because it is not an independent design parameter. The essential quantity is the solidity of the blading which is also influenced by the chord length. As outlined below, the chord length is a free design parameter wherefore it is possible to obtain arbitrary solidities along the blade span even though the number of blades is constant.

- Free Optimization Parameters

- One essential optimization parameter has no impact on reversibility: The the hub-to-tip ratio. Large hub-to-tip ratios increase the kinetic energy associated with the through-flow velocity and hence decrease the total-to-static efficiency. Small hub-to-tip ratios, however, favor secondary flows and hence friction losses. Initial values for the optimization process were obtained from classical empirical recommendations according to Strscheletzky and de Haller [5, 6].
- While the blade sections must be non-cambered, their chord length and stagger angle (i.e. rotor plane and the blade chord) may vary in spanwise direction - without compromising reversibility. For the present study, these parameters where discretized at five equidistant stations between hub and tip and a spline curve was used to obtain a continuous distribution over the blade height. Optimization of the chord length and the stagger angle eventually yields an optimal spanwise aerodynamic loading distribution. The initial chord length was 10 mm (12.5 % of the diameter). The stagger angle was initialized such that the angle of attack amounts to  $5^\circ$  throughout the blade height.
- The rotational speed of the second impeller, in other words the ratio of rotational speeds of downstream (“A”) and upstream (“B”) impeller

$$z \equiv n_B / n_A, \quad (2)$$

was optimized, too. Of course, the final fan can be operated at various speed ratios, but the geometry will only be optimal for the one speed ratio obtained in the optimization process. In summary, there are twelve free optimization parameters: the hub-to-tip ratio, the speed ratio, the chord length at five spanwise locations and the stagger angle at five spanwise locations.

## CFD Model

The CFD model is utilized to evaluate the objective function, i.e. the total-to-static efficiency. The two impellers are placed in a cylindrical duct-type housing with a diameter equal to the nominal fan diameter. The housing starts one fan diameter upstream of the upstream impeller and ends one fan

diameter downstream of the downstream impeller. The flow in only one blade channel is simulated assuming rotational periodicity at the lateral boundaries. This computational domain is discretized with the open source mesh generator cfMesh (2018 release) using approximately two million cells (i.e. one million per impeller). Since the number of blades is identical for both impellers, there is no need for an interface in between.

In order to keep the computational cost to an affordable level, only steady-state Reynolds-averaged Navier-Stokes (RANS) flow simulations are carried out, performed with the open source code OpenFOAM (2016 release). In spite of the relatively low blade chord based Reynolds number fully turbulent flow is assumed and modelled with the Shear Stress Transport (SST) turbulence model. The multi-reference-frame (MRM) model is used to incorporate the distinct rotational speeds of the two stages.

The design flow rate is prescribed at the inlet and ambient pressure is prescribed at the outlet. No-slip boundary conditions are set at all walls (blade, hub, shroud).

## EXPERIMENTAL SET-UP AND DATA EVALUATION

The fan assembly is depicted in Fig. 4. The hub of each impeller houses a small electronically commutated Brushless Direct Current Motor BLDC with a maximum power of 55 W (Hacker® type A10S-15). Both motors are mounted in the duct type housing via three radial struts with circular cross-section.

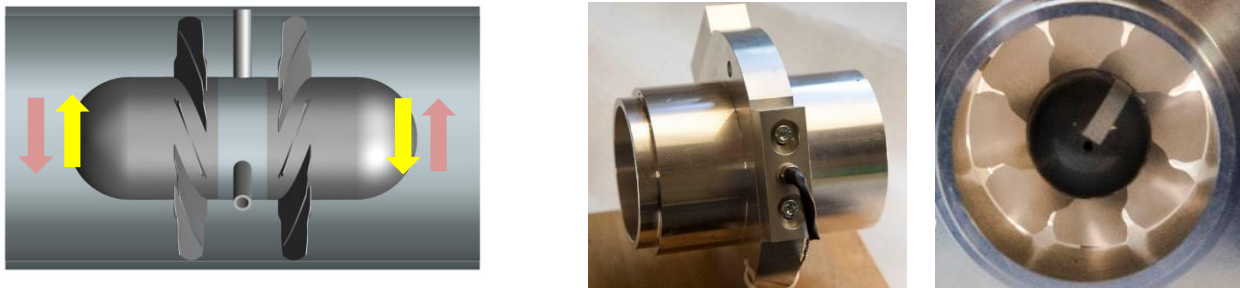


**Figure 4:** Fan assembly: The two contra-rotating rotors in a duct type housing.

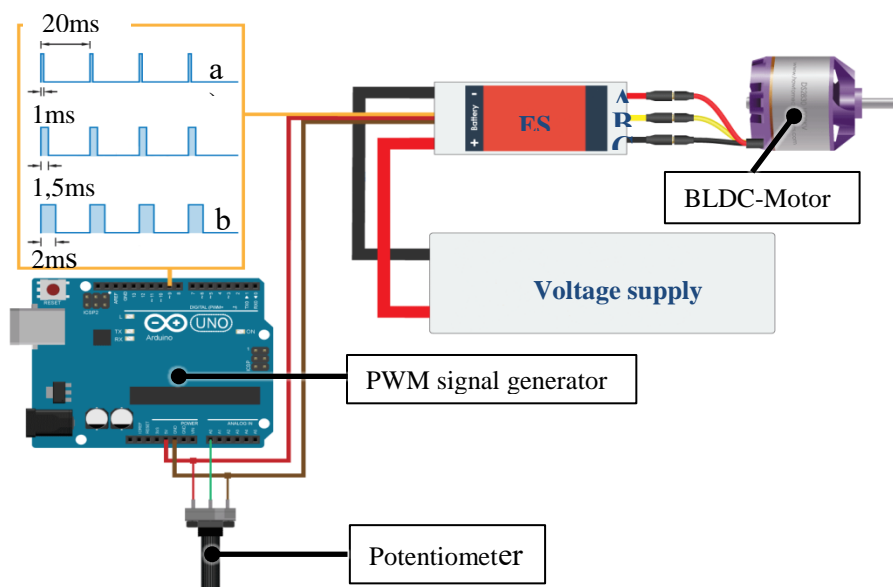


**Figure 5:** Complete drive train for one impeller; pulse width a) for minimum and b) maximum rotational speed, [7].

The rotational speed of each motor is controlled manually with a potentiometer. An Arduino™ board [7] is used to translate the position of the potentiometer into a 50 Hz pulse width modulated (PWM) signal which is fed into the Electronic Speed Controller ESC (Hacker® type X5), Fig. 5.

The fan assembly is mounted to a standard suction side chamber fan test rig, where the characteristic curves are determined experimentally. A bell mouth inlet nozzle is attached to the active inlet. The pressure rise coefficient is defined as

$$\psi_{ts} \equiv \Delta p_{ts} / \left( \frac{\pi^2}{2} \rho D^2 n_A^2 \right). \quad (3)$$

where  $\Delta p_{ts}$  is the total-to static pressure rise of the complete assembly. The total-to static aerodynamic efficiency  $\eta_{ts}$  cannot be measured because of the lack of an accurate micro-torque meter. Instead, as an estimate the electric efficiency is taken:

$$\eta_{el} \equiv \frac{\dot{V} \Delta p_{ts}}{P_{el} - P_{el,controller}} = \frac{\dot{V} \Delta p_{ts}}{UI - U_0 I_0}. \quad (4)$$

$P_{el,controller}$  is the electric power consumed by the controller and the motors with both impellers removed.

## RESULTS

One of the resulting optimized impellers is shown in Fig. 6. Remarkable is the spanwise chord distribution, which results in a wavy blade leading and trailing edge. In general, the solidity is rather large. The tip gap-to-impeller diameter ratio for all experiments is 0.3 %.

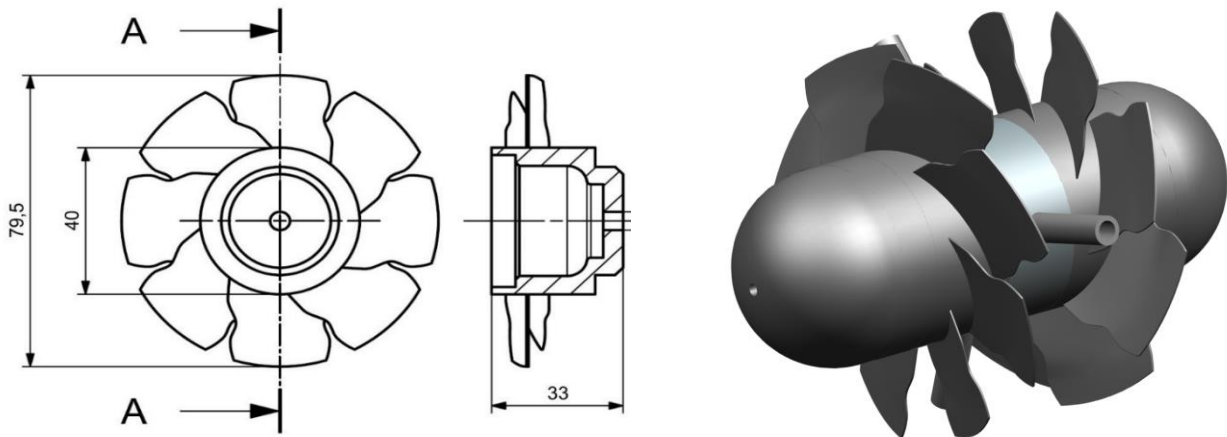


**Figure 6:** Left: Optimized impeller, right: The assembly of the two contra-rotating impellers

The predicted optimal rotational speed ratio is  $z_{opt} = 0.825$  which yields a predicted  $\psi_{ts,opt} = 0.50$  at  $\phi_{opt} = 0.10$ . This optimal pressure coefficient is rather high which was expected since a higher pressure rise coefficient usually correlates with a higher static share in the total pressure.

These operational values are perfectly validated by the measurements, Fig. 7. An interesting experimental result is that for  $\phi > 0.10$  a value for the ratio  $z \rightarrow 1$  yields even a higher efficiency, But this was not investigated within the optimization. It is important to remember that the electric efficiency is only a coarse estimate of the true total-to-static efficiency. Hence, conclusions from the efficiency characteristic have to be drawn with some caution.

Interesting is the question how the fully reversible contra-rotating fan compares to the state-of-the-art single-stage impeller-only axial fans. The coloured surface in Fig. 8 reflects the performance of the class of single-stage impeller-only axial with maximum possible efficiency. This information was obtained by an extended study of such fans by Bamberger [8, 9]. The fully reversible contra-rotating fan produces a comparably large total-to-static pressure rise at a comparably low volume flow rate. As such it is rated a high pressure axial fan. This comes at no surprise: The contra-rotating downstream impeller not only acts as a stator but feeds in additional energy into to fluid.

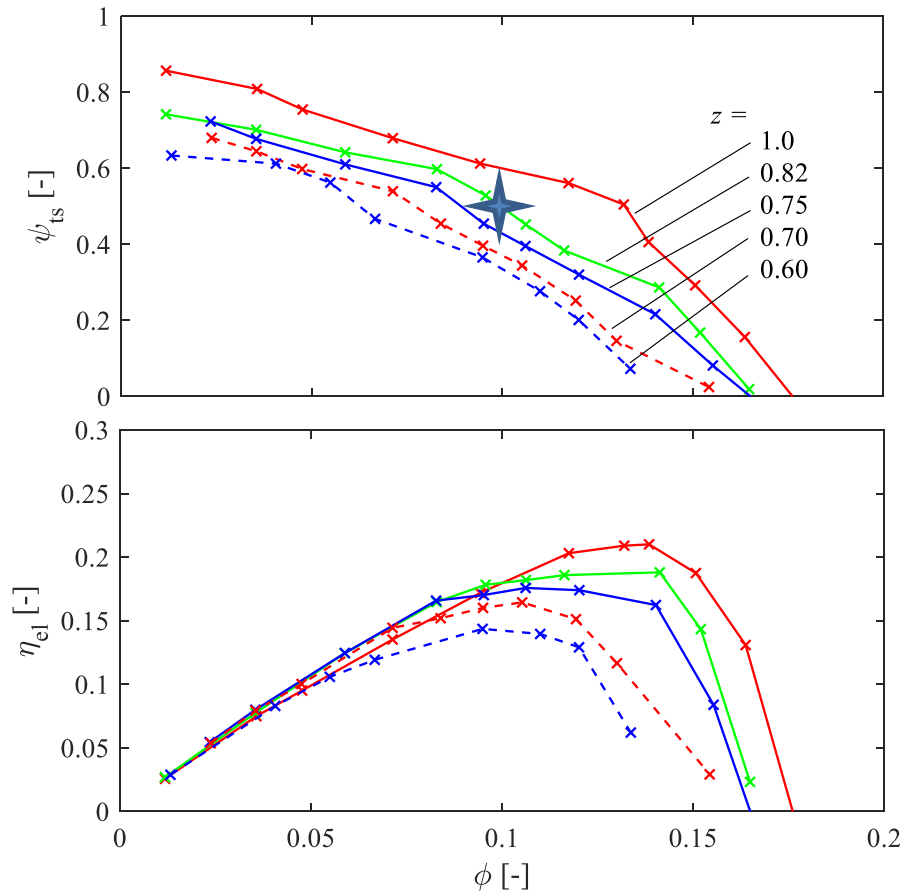


**Figure 7:** Measured performance characteristics for various speed ratios  $z$ ;  $n_A = 4000$  rpm; the star indicates the CFD-predicted operating point for the predicted optimal rotational speed ratio  $z_{opt} = 0.825$ .

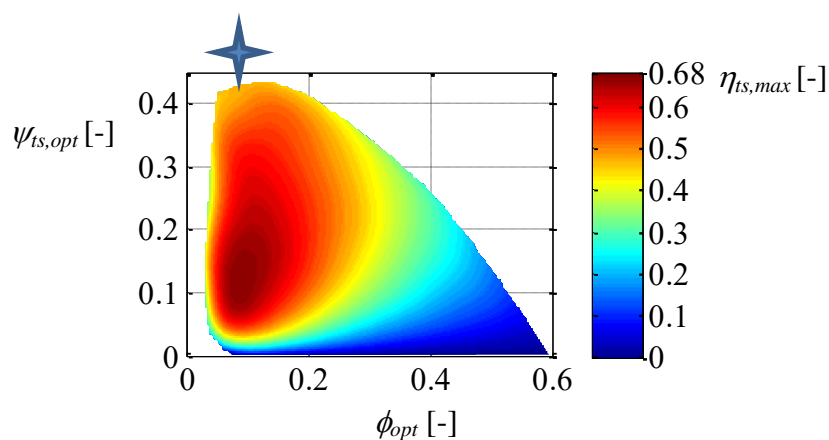


**Figure 8:** Performance of the class of single-stage impeller-only axial fans; the star indicates values from the fully reversible contra-rotating fan as in Fig. 7, from Bamberger [8].

Finally, Fig. 9 visualizes the velocity field at the fan exit, i.e. in a plane close to the exit of the downstream impeller. As expected the swirl disappears for a speed ratio of  $z \approx 1$  which corresponds to the highest values of pressure rise coefficient and efficiency.

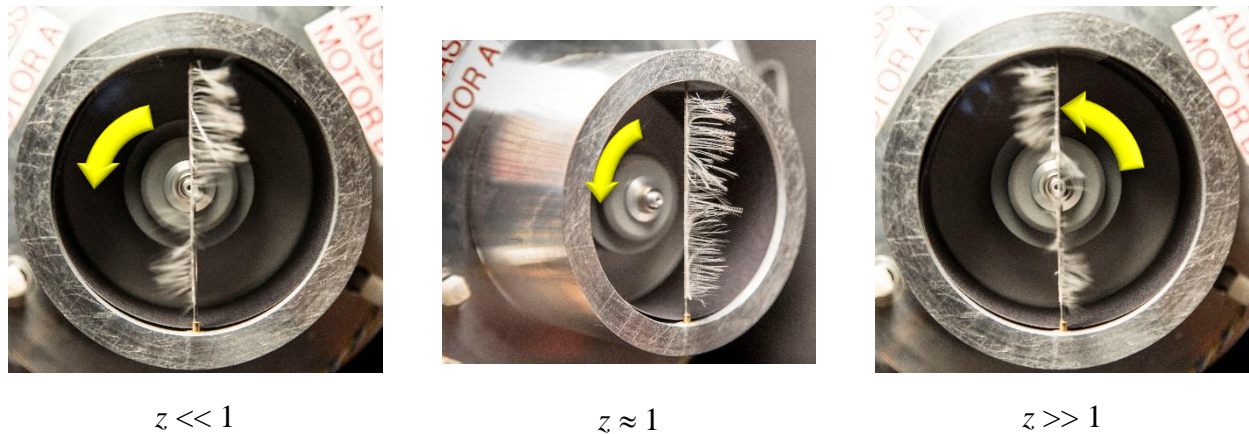


**Figure 9:** Visualization of the swirling flow at the exit of the downstream impeller as a function of speed ratio; the yellow arrow indicates the sense of rotation of the downstream impeller, whereas the upstream impeller rotates in the opposite direction with constant rotational speed  $n_A$ ; the threads in the center indicate the wake behind the hub.

There is a concern for excessive noise emission from fans with contra-rotating impellers. The interaction of the eight-bladed impellers with the three struts and the interaction of the blades of the upstream with the downstream impeller are candidates for tonal noise generators. The consequence of this multiple interaction is a large number of circumferential pressure modes which may be propagating or be cut-off. Fig. 10 shows a narrow band sound pressure spectrum measured in the vicinity of the fan assembly. The fan was operated with  $n_A = n_B = 4000$  rpm ( $z = 1.0$ ) at  $\phi = 0.10$ . The tonal peaks at shaft rotating frequency  $SRF = n$  [rpm]/60 are probably attributed to an imperfect balancing of the both impellers. The dominant peak and most annoying tone is observed at twice the blade passing frequency  $BPF = zn$  [rpm]/60. This is expected since both 8-blades impellers rotate with 4000 rpm each, i.e. the relative rotation is at 8000 rpm. It is important noting that - from an acoustic perspective - the choice of the same number of blades for each impeller is unfavourable. An acoustically advanced design would consist of two impellers with different blade numbers. To what degree this impairs *full* reversibility needs to be investigated.

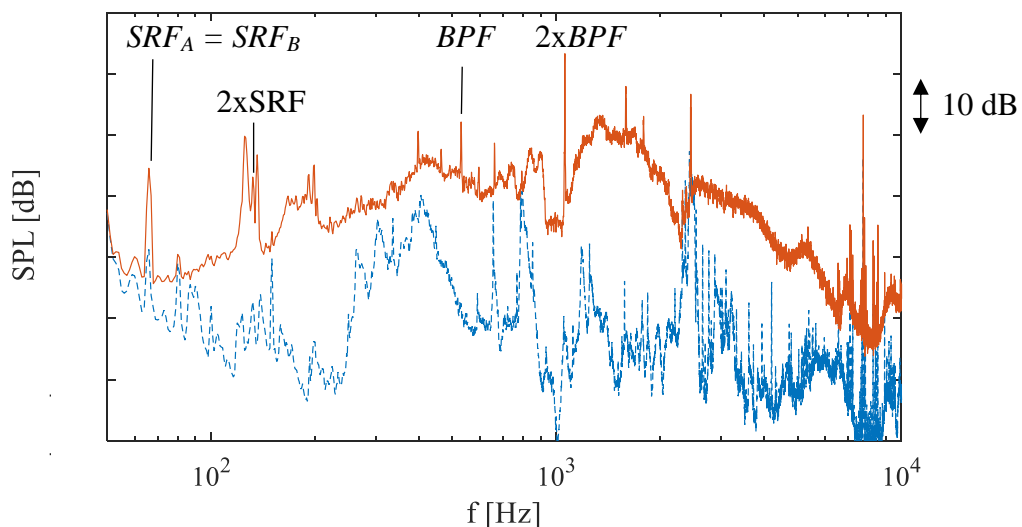


**Figure 10:** Red: Narrow band sound pressure spectrum in the vicinity of the fan assembly operating with  $n_A = n_B = 4000$  rpm  $z = 1.0$  at  $\phi = 0.10$ ; blue dashed: dito but impellers removed (background noise).

## SUMMARY AND CONCLUSIONS

Within this study a small version of a fully reversible fan was designed. *Reversibility* is achieved by reversing the rotational speed, *full* reversibility by symmetric impellers with non-cambered blades. The disadvantage of non-cambered blades with respect to pressure rise are compensated by the choice of two identical contra-rotating impellers. The optimal geometry and speed ratio was found by a CFD-based optimization. The resulting fan is characterized by a high value of the pressure rise coefficient, superior to a standard non-reversible rotor-only fan. Of course the fan assembly requires a second motor which increases cost. Although the most favorite ratio of up- and downstream impeller rotational speed is close to 1, an independent speed control of both motors allows full control of the characteristic performance curves - for both flow directions.

The CFD-predicted performance data agree well with experimental data. The optimized contra-rotating fan is believed to be superior to state-of-the art designs known from the literature.

The interaction of the eight-bladed impellers with the three struts and the interaction of the blades of the upstream with the downstream impeller are responsible for distinct tones observed in the measured sound pressure spectrum. An acoustically advanced design would consist of two impellers with different blade numbers. To what degree this impairs *full* reversibility needs then to be investigated.

As an outlook several of these contra-rotating impeller assemblies could be placed in one duct without guide vanes in order to increase the pressure rise even further while maintaining full reversibility.

## BIBLIOGRAPHY

- [1] <http://cleanfix.org/de/produkte/cleanfix-sc>, accessed Nov 09, **2021**
- [2] C. Kramer and R. Grundmann – *Reversierbarer Strömungsantrieb*. German patent DE 3938975 C1, Nov 24, **1989**
- [3] B. Eck – *Ventilatoren*. Springer-Verlag, Berlin-Heidelberg, **1972**
- [4] J. A. Nelder and R. Mead – *A Simplex Method for Function Minimization*. Computer Journal, 7, pp. 308-313. **1965**
- [5] J. H. Horlock – *Axialkompressoren*. Verlag G. Braun, Karlsruhe, **1967**
- [6] P. de Haller – *Das Verhalten von Tragflügelgittern in Axialverdichtern und im Windkanal*. Brennstoff-Wärme-Kraft, Bd. 5, Heft 10, **1953**, pp. 333–337
- [7] <https://howtomechatronics.com>: Arduino Brushless Motor Control Tutorial | ESC | BLDC - HowToMechatronics, **2019**. <https://howtomechatronics.com/tutorials/arduino/arduino-brushless-motor-control-tutorial-esc-bldc/>, accessed Feb. 11, 2020
- [8] K. Bamberger – *Aerodynamic optimization of low-pressure axial fans*. Shaker Verlag **2015**, ISBN 978-3-8440-4031-9; doi: 10.2370/9783844040319
- [9] K. Bamberger and T. Carolus – *Development, Application, and Validation of a Quick Optimization Method for the Class of Axial Fans*. ASME Journal of Turbomachinery, Nov **2017**, Vol. 139; doi.org/10.1115/1.4036764